A Three-Dimensional Spatial Mapping Approach to Quantify Fine-Scale Heterogeneity Among Leaves within Canopies

Authors: Wingfield, Jenna L., Ruane, Lauren G., and Patterson, Joshua D.

Source: Applications in Plant Sciences, 5(11)

Published By: Botanical Society of America

URL: https://doi.org/10.3732/apps.1700056

Applications in Plant Sciences

Applications in Plant Sciences 2017 5(11): 1700056

Application Article

A three-dimensional spatial mapping approach to quantify fine-scale heterogeneity among leaves within canopies[1]

Jenna L. Wingfield[2], Lauren G. Ruane[3], and Joshua D. Patterson[2,4]

[2]Department of Molecular Biology and Chemistry, Christopher Newport University, Newport News, Virginia 23606 USA; and
[3]Department of Organismal and Environmental Biology, Christopher Newport University, Newport News, Virginia 23606 USA

- *Premise of the study:* The three-dimensional structure of tree canopies creates environmental heterogeneity, which can differentially influence the chemistry, morphology, physiology, and/or phenology of leaves. Previous studies that subdivide canopy leaves into broad categories (i.e., "upper/lower") fail to capture the differences in microenvironments experienced by leaves throughout the three-dimensional space of a canopy.
- *Methods:* We use a three-dimensional spatial mapping approach based on spherical polar coordinates to examine the fine-scale spatial distributions of photosynthetically active radiation (PAR) and the concentration of ultraviolet (UV)-absorbing compounds (A_{300}) among leaves within the canopies of black mangroves (*Avicennia germinans*).
- *Results:* Linear regressions revealed that interior leaves received less PAR and produced fewer UV-absorbing compounds than leaves on the exterior of the canopy. By allocating more UV-absorbing compounds to the leaves on the exterior of the canopy, black mangroves may be maximizing UV-protection while minimizing biosynthesis of UV-absorbing compounds.
- *Discussion:* Three-dimensional spatial mapping provides an inexpensive and portable method to detect fine-scale differences in environmental and biological traits within canopies. We used it to understand the relationship between PAR and A_{300}, but the same approach can also be used to identify traits associated with the spatial distribution of herbivores, pollinators, and pathogens.

Key words: *Avicennia germinans*; spatial mapping; spherical polar coordinates; UV-absorbing compounds.

Plants are able to survive a variety of environmental conditions due in part to their ability to detect and respond to their environment. Although ultraviolet (UV) light has the potential to damage DNA and photosynthetic machinery, plants can minimize its negative effects by synthesizing UV-absorbing compounds (Li et al., 1993; Landry et al., 1995) such as flavonoids, hydroxycinnamic acids (HCAs), and mycosporine-like amino acids (Beggs and Wellmann, 1994; Cockell and Knowland, 1999; Agati et al., 2013). These phenolic secondary metabolites can protect plants from UV damage by decreasing the transmittance of UV photons through tissue. Given that UV-absorbing compounds are energetically expensive to produce (Weinig et al., 2004), most plant species plastically upregulate their production in response to UV-exposure (Lois, 1994; Dixon and Paiva, 1995). When these compounds are energetically expensive yet adaptive (i.e., when they increase fitness in the presence of UV, but decrease fitness in the absence of UV), natural selection will favor individuals that optimally allocate these compounds to cells that shield valuable tissues from UV exposure (Weinig et al., 2004). For example, UV-absorbing compounds are concentrated within trichomes and/or epidermal cells on the adaxial surface of leaves, which decreases the transmittance of UV-light into the mesophyll cells beneath (Cen and Bornman, 1993; Reuber et al., 1996; Schnitzler et al., 1996; Burchard et al., 2000; Tattini et al., 2000; Bilger et al., 2001; Agati et al., 2002). The reduction in epidermal transmittance in turn reduces damage to photosynthetic machinery (Tevini et al., 1991; Kolb et al., 2001) and DNA (Mazza et al., 2000). There is also evidence that plants nonrandomly distribute UV-absorbing compounds within their reproductive organs (Day and Demchik, 1996a, 1996b) and seeds (Griffen et al., 2004).

The concentration of UV-absorbing compounds may also vary among leaves within canopies. Previous studies have subdivided leaves into broad categories (i.e., "unshaded vs. shaded" or "upper vs. lower canopy") and found higher concentrations of UV-absorbing compounds in "unshaded" or "upper" leaves (Lovelock et al., 1992; McKee, 1995). However, using categorical variables to quantify leaf position does not sufficiently capture the differences in microenvironments experienced by leaves throughout the entire three-dimensional space of a canopy. For example, leaves on the exterior of canopies alter both the quantity

[1]Manuscript received 26 May 2017; revision accepted 30 September 2017.

The authors thank V. Bernhard and his family for supporting undergraduate research and for allowing access to the collection sites, Shane Heschel for providing statistical advice, and Rachel Cochrane for providing an artistic rendering of the canopy. Funding was provided by the Hummingbird Cay Foundation, the Honors Program, the Department of Organismal and Environmental Biology, and the Department of Molecular Biology and Chemistry at Christopher Newport University.

[4]Author for correspondence: joshua.patterson@cnu.edu

doi:10.3732/apps.1700056

and quality of light received by leaves on the interior of canopies (Le Roux et al., 2001; Baldocchi et al., 2002; Valladares, 2003). Although multiple methods exist for quantifying leaf position within a canopy, they are often challenging to implement due to both financial and/or logistical constraints in the field. For example, digitizing methods (i.e., sound propagation: Sinoquet et al., 1991; Room et al., 1996; magnetic field current induction: Sinoquet et al., 1998; Le Roux et al., 2001; Everhart et al., 2011; and LiDAR: Greaves et al., 2015; Magney et al., 2016; Swatantran et al., 2016) are expensive, require electrical power supplies, and fail to access the inner canopy (Magney et al., 2016). Moreover, digitizing methods generate enormous data sets that often require discrete variable distinctions such as flush numbering, stem and branch classifications, or primary and lateral leaf groups to clearly observe trends within the canopy (Sinoquet et al., 1998).

We introduce a simple, inexpensive, and portable method based on a spherical polar coordinate system to quantify the exact location of leaves within the canopy of black mangrove (*Avicennia germinans* (L.) Stearn) trees. By quantifying leaf position with three continuous variables (radial distance, zenith angle, and azimuthal angle) and a set of mathematical combination variables (radial and vertical canopy depths), we are able to use linear regressions to determine how light quantity changes throughout the canopy and how leaf position within the canopy affects the concentration of UV-absorbing compounds. Black mangrove trees were selected for this study for several reasons. First, as inhabitants of the tropics, black mangroves receive higher levels of UV radiation than plants inhabiting temperate regions (Frederick et al., 1989; Madronich, 1993). Moreover, this species inhabits coastlines and is rarely shaded by taller trees. Consequently, black mangroves have had the opportunity to adapt to this high-UV environment by evolving strategies that minimize UV damage (Lovelock et al., 1992; Weinig et al., 2004). Black mangrove trees are also an ideal species because their canopies are large enough to create a multitude of microenvironments, but small enough to sample thoroughly.

MATERIALS AND METHODS

***Plant system*—**The four black mangrove (*A. germinans*) trees included in our study were of similar sizes and occurred as single isolated trees along the beach on the west side of Hummingbird Cay, a privately owned island located approximately 13 km west of Georgetown in the Great Exuma island chain of the Bahamas. Geospatial coordinates for the trees are as follows: (23°27′35.2800″N, 75°56′39.8040″W), (23°27′36.8640″N, 75°56′39.5520″W), (23°27′37.2168″N, 75°56′39.8148″W), and (23°27′43.1964″N, 75°56′39.8256″W).

***Quantifying leaf position using spherical polar coordinates*—**A spherical polar coordinate system was used to quantify the spatial location of 49–50 leaves within each canopy. This coordinate system uses three continuous variables (ρ, θ, φ) to specify leaf location. Approximately 12 leaf samples were collected per quadrant of each canopy, which yielded spatial locations with many combinations of ρ, θ, and φ. ρ is the radial distance or the direct distance of a point from a fixed origin, θ is the zenith angle measured from a fixed vertical direction, and φ is the azimuthal angle, measured as the angle relative to a fixed direction on a reference plane that passes through the origin and is orthogonal to the vertical direction (Fig. 1). The origin is defined as the trunk of the tree at the base of the canopy. Radial distance (ρ) was measured by looping a piece of twine around the trunk of the tree at the base of the canopy. A flexible tape measure was then secured to the twine with 0 cm positioned at the base of the canopy. The twine was drawn to the center of the leaf location, and the direct distance from the trunk to the leaf was measured to the nearest centimeter.

To measure the angular components (θ, φ) of the spatial location, two measurement protractors were prepared from printed 360° protractor images. The protractors were secured to two layers of folder stock, cut to shape, and then laminated. Materials were selected on the basis of availability, ease of construction, and field-portability. The protractor used to measure zenith angle (θ) was prepared by cutting the first 360° protractor in half along the 0° line. A second cut (~55 mm) was made, originating from the flat end of the corresponding 180° protractor, along the 90° line (Appendix 1). The protractor was positioned such that the flat edge was flush with the tree trunk and 0° was oriented directly vertical. Measurements were recorded to the nearest degree (with a spacing of 1.75 mm per degree) and ranged from 0–90°. The protractor used to measure azimuthal angle (φ) was prepared using the second 360° protractor. A ~100 mm cut was made along the 0° line toward the center of the protractor. Three additional cuts (~55 mm) originating from the origin of the protractor were made along the 90°, 180°, and 270° lines (Appendix 2). The single long cut allowed the protractor to be pulled around the base of the canopy, and the three shorter cuts provided space to position the base of the canopy at the origin. The protractor was then secured, leveled using a bubble level, and oriented with 0° positioned at due north using a compass. Measurements of φ were recorded to the nearest degree and ranged from 0–360°. The 180° zenith protractor was fitted perpendicular to the azimuthal protractor using the partial cut along 90° line of the zenith protractor (Appendix 3). The angular coordinates were measured using the direct path of the twine to the leaf location relative to the two protractors. Using this method, we are able to spatially map the canopy at the resolution scale of individual leaves. Measurement errors in ρ, θ, and φ are ±1 cm, ±1°, and ±1°, respectively, and are below the scale of individual leaves.

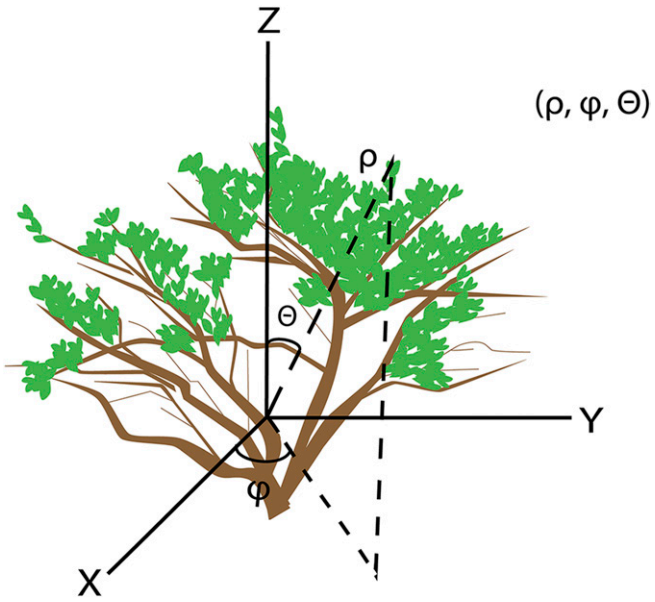

Fig. 1. Visual depiction of the spherical polar coordinate system used to quantify the spatial location of each leaf sampled. ρ is the direct distance of a point from a fixed origin, θ is the zenith angle measured from a fixed vertical direction, and φ is the azimuthal angle, measured as the angle relative to a fixed direction on a reference plane that passes through the origin and is orthogonal to the vertical direction.

***Quantifying PAR and UV-absorbing compounds*—**After measuring the spherical polar coordinates of each leaf, the amount of photosynthetically active radiation (PAR) it received was determined by placing the sensor of a handheld light meter (LI-250; LI-COR, Lincoln, Nebraska, USA) at the adaxial leaf surface. To minimize variation in full sun (unobstructed by leaves) PAR, we only collected data between 12:00 p.m. and 3:00 p.m. on sunny days and we sampled all 49–50 leaves within a single canopy on the same day. Full sun PAR during data collection ranged from 1566 to 1719 μmol m^{-2} s^{-1}. Collecting data from a subset of leaves from each tree each day would have required that we spend more time sampling each day and consequently would have increased the range of full sun PAR levels during sampling.

Following the measurement of PAR, a leaf disk (31.2 mm^2) was collected from the middle of the leaf at its widest part using a cork borer. Disks were placed in individual 5-mL Eppendorf tubes containing 4 mL of a 90 : 1 : 1

methanol : HCl : H_2O (v : v : v) extraction solution prepared from methanol (Thermo Fisher Scientific, Waltham, Massachusetts, USA), concentrated HCl (37% HCl; Sigma-Aldrich, St. Louis, Missouri, USA), and deionized H_2O (Griffen et al., 2004). Tubes were covered in aluminum, stored at −3°C, and then transported to the laboratory. Aliquots (200 µL) of each leaf extraction solution were then diluted to total volumes of 2000 µL using the 90 : 1 : 1 methanol : HCl : H_2O solution. The concentration of UV-absorbing compounds in each leaf sample was quantified by measuring absorption at 300 nm (A_{300}) using a UV-Vis spectrometer (Shimadzu UVmini-1240; Shimadzu Corporation, Kyoto, Japan).

***Analyses*—**Although the four black mangroves included in our study were similarly sized, the maximum value of ρ differed among trees. Thus, we standardized this variable by dividing the value of ρ for each leaf within a tree data set by the maximum value of ρ within the data set. In this framework, the maximum ρ for each tree was 1.0 or 100%ρ. The new variable (%ρ) was then used in all calculations of canopy depth. Because φ and θ were oriented to global directions, 0° at due north and 0° at vertical, respectively, the angular measurements of individual trees could be combined into a single data set. Measurements in φ were converted to radians and transformed from circular to linear variables using a sine function.

We quantified leaf position by calculating radial (R_D) and vertical (V_D) canopy depths, continuous variables that indicate the thickness of the canopy along the vector formed by θ and directly above each sampled leaf, respectively (Fig. 2). Essentially, V_D is the quantitative analog of the coarser distinctions of "upper"/"lower" or "shaded"/"unshaded" canopy leaves, and measures the vertical distance from the canopy exterior to a leaf sample. The expressions for R_D and V_D were derived by approximating the exterior of the tree canopy as a hemisphere with an arc of radius 100%ρ. R_D was calculated as the direct distance from the canopy exterior to the leaf along θ as:

$$R_D = 100\%\rho - \%\rho$$

For V_D a pair of overlapping right triangles with bases of identical lengths and hypotenuses of 100%ρ and %ρ were used to determine the total thickness of the canopy and the thickness below the leaf position, respectively. V_D was calculated as the difference between these thicknesses using trigonometric identities and the values of 100%ρ, R_D, and θ as follows:

$$V_D = \sqrt{(100\%\rho)^2 - ((100\%\rho - R_D)\cdot \sin(\theta))^2} - (100\%\rho - R_D)\cdot\cos(\theta)$$

Vertical canopy depths ranged from a minimum value of 0%ρ (for leaves located on the exterior of the canopy) to a maximum of 100%ρ (for leaves at the base of the canopy with $\theta = 0°$).

Multiple linear regressions were used to determine the effects of V_D, R_D, θ, and φ on PAR and A_{300}. Fixed effects of R_D, θ, φ, V_D, as well as interactions between the spatial variables (R_D, θ, φ), were examined with tree identity treated as a random effect. Analyses of residuals revealed that model errors were normally distributed and variances were homogenous. All variance inflation factors were less than 1.08, indicating that correlations between variables defining leaf location (R_D, θ, φ) were weak. The relationships between the predictors and the response variables in our data set were linear; other statistical analyses could be adopted if the relationships between variables are nonlinear.

Analyses were performed using JMP version 9.0 (SAS Institute, Cary, North Carolina, USA). Results are considered to be significant when $P < 0.05$. Three-dimensional spatial visualization was performed using MATLAB version 2015a (MathWorks, Natick, Massachusetts, USA). Spherical polar coordinates were converted to a Cartesian coordinate system for ease of visualization using the following formulas:

$$x = \%\rho\sin(\theta)\cos(\varphi)$$

$$y = \%\rho\sin(\theta)\sin(\varphi)$$

$$z = \%\rho\cos(\theta)$$

PAR and A_{300} were plotted as color gradient scatter plots on a unitless Cartesian coordinate scale.

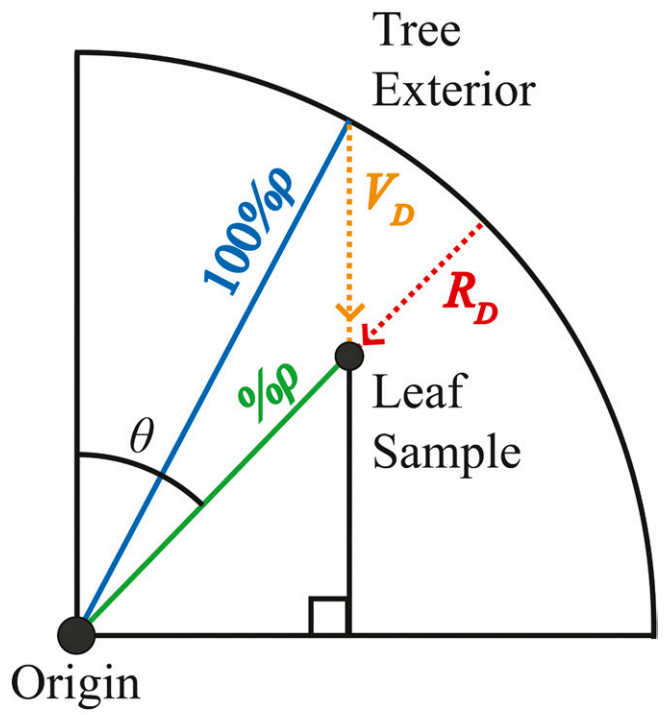

Fig. 2. Schematic illustrating radial canopy depth (R_D) and the trigonometric approximation of vertical canopy depth (V_D).

RESULTS

***Spatial distribution of PAR*—**The amount of PAR received by the leaves ranged from 76.5 to 1718.7 µmol m^{-2} s^{-1} and depended on the leaf position (Table 1, Fig. 3A). Overall, leaves on the exterior of the canopy received more PAR than leaves on the interior. Although PAR was negatively correlated with R_D ($\beta = -10.6088$, $P < 0.0001$), it was not significantly correlated with the other spatial variables θ and φ or any interaction term combinations of the spatial variables (Table 1). The strong dependence of PAR on R_D is consistent with an internal shading model within the canopy, where the pigments within outer leaves reduce the amount of radiation that reaches the interior leaves.

***Spatial distribution of UV-absorbing compound concentrations (A_{300})*—**The concentration of UV-absorbing compounds varied among leaves throughout the canopy (i.e., individual A_{300} values ranged from 0.301 to 1.089). This variation was explained in part by the position of the leaf within the canopy (Table 1, Fig. 3B). Much like the observed spatial trends in PAR, A_{300} was negatively correlated with R_D; leaves at the exterior of the tree canopy contained higher concentrations of UV-absorbing compounds than leaves on the interior of the canopy ($\beta = -0.0041$, $P < 0.0001$). Also similar to PAR, A_{300} was not significantly correlated with any of the other spatial variables or the interaction terms.

***Vertical canopy depth (V_D)*—**Both PAR and A_{300} were negatively correlated with V_D ($P < 0.0001$; Table 2). To understand this observation, we examined the independent spatial variables that can contribute to V_D (i.e., R_D and θ). Although PAR and A_{300}

TABLE 1. Results of multiple linear regression models showing the effects of independent variables on PAR and A_{300} in *Avicennia germinans*.

	PAR			A_{300}		
Independent variable	β[a]	SE	P	β[a]	SE	P
Radial depth (R_D)	−10.6088	1.9144	<0.0001*	−0.0041	0.0008	<0.0001*
Zenith angle (θ)	−10.7952	95.8039	0.9105	−0.0483	0.0384	0.2136
Azimuthal angle (φ)	−71.7041	44.2598	0.1069	−0.0268	0.0176	0.1292
(R_D) · (θ)	−4.5004	5.4300	0.4083	0.0041	0.0022	0.0556
(R_D) · (φ)	0.4470	2.7059	0.8690	−0.0008	0.0011	0.4801
(θ) · (φ)	183.6539	115.9051	0.1147	0.0878	0.0459	0.0571
(R_D) · (θ) · (φ)	−3.5184	7.8847	0.6559	0.0007	0.0031	0.8304

[a]A negative β (standardized coefficient) indicates a negative relationship between the independent and dependent variables.
*Indicate significant values ($P < 0.05$).

were both correlated with R_D, neither showed a significant correlation with θ or the $R_D \cdot \theta$ interaction term in the linear regression analysis, indicating that the effect of R_D on PAR and A_{300} was independent of θ. Consequently, the observed correlation of PAR and A_{300} with V_D was driven by R_D and was not significantly influenced by θ.

DISCUSSION

We have developed a simple, economical, and portable method based on a spherical polar coordinate system to quantify the exact location of leaves within the canopy. By defining leaf position with three continuous variables in spherical coordinates, our three-dimensional spatial mapping technique can detect fine-scale heterogeneity in both environmental conditions (i.e., PAR) and biological traits (i.e., A_{300}) throughout the entire canopy of individual trees. Data collected using this method can be analyzed using multiple linear regressions to determine the degree to which each spatial variable (i.e., R_D, θ, and φ) and combination of spatial variables (i.e., their interaction terms) explain the variation observed.

In our application of this method, we found that the spatial variation in both PAR and A_{300} within the canopy of black mangrove (*A. germinans*) trees was due to R_D. The shared R_D-dependence of PAR and A_{300} suggests that the spatial distribution of light within canopies could determine the spatial distribution of UV-absorbing compounds. Multiple studies have observed increased production of photoprotective flavonoids and HCAs upon increased light exposure for plant species of diverse geographical origins (McKee, 1995; Schnitzler et al., 1996; Tegelberg et al., 2001; Izaguirre et al., 2007; Sullivan et al., 2007; El Morchid et al., 2014; Nascimento et al., 2015). In a manipulative growth chamber experiment, black mangrove seedlings grown in high light (339 ± 4 µmol m^{-2} s^{-1}) had 52% more phenolics than those grown in low light (37 ± 1 µmol m^{-2} s^{-1}) (McKee, 1995). The observed significant negative correlations of PAR and A_{300} with R_D in our study suggest that the light microenvironment and the biosynthesis of UV-absorbing compounds are also coupled in adult trees in the field. Moreover, these results provide a plausible framework for explaining how the canopy distributes UV-absorbing compounds. Rather than produce a uniform concentration of UV-absorbing compounds across the entirety of the canopy, black mangroves preferentially allocate more UV-absorbing compounds to the outermost leaves, which receive more incoming solar radiation.

Other methods have been used to quantify the fine-scale environmental and biological heterogeneity within canopies. For example, leaf position has been quantified using leaf area index (Hirose and Werger, 1987; Pierce and Running, 1988; Ellsworth and Reich, 1993; Bréda, 2003; Weiss et al., 2004; Li et al., 2014; Magney et al., 2016) and vertical canopy depth (Ellsworth and Reich, 1993; Sinoquet et al., 1998; Magney et al., 2016). However, leaf area index methods often require either direct harvesting

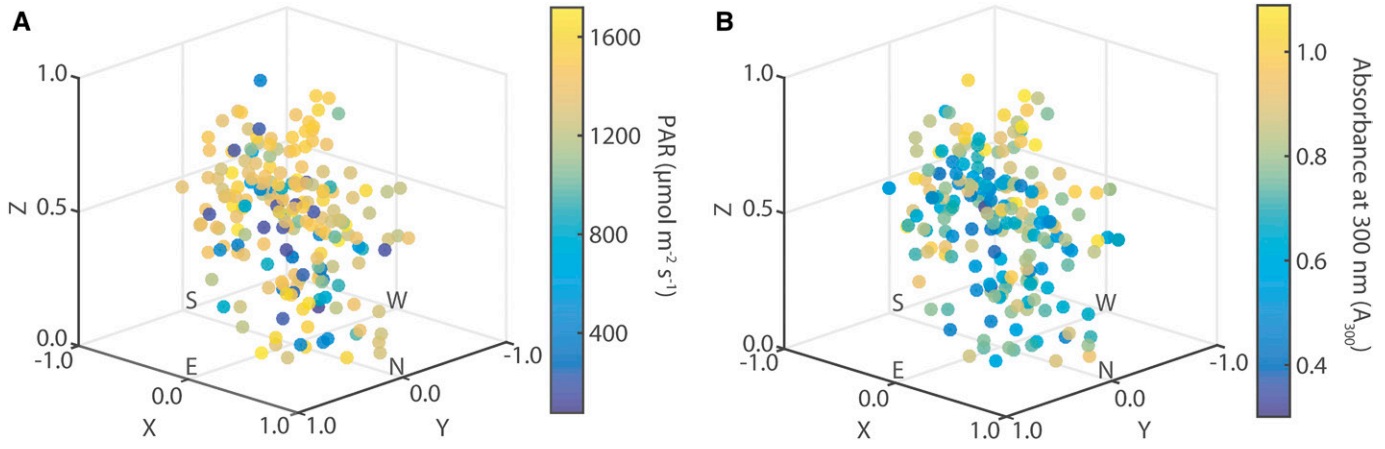

Fig. 3. Three-dimensional spatial distribution of (A) photosynthetically active radiation (PAR) and (B) UV-absorbing compound concentration as indicated by the absorbance at 300 nm (A_{300}) within the canopy based on the combined leaf measurements from four black mangrove (*Avicennia germinans*) trees on a unitless Cartesian scale. Orientation of the composite canopy relative to the cardinal directions is displayed along the *x*-*y* plane.

TABLE 2. Results of linear regression models showing the effects of vertical depth (V_D) on PAR and A_{300} in *Avicennia germinans*. V_D is the quantitative analog of existing coarse descriptions of "upper" and "lower" canopies.

	Vertical depth (V_D)		
Dependent variable	β[a]	SE	P
PAR	−7.8395	1.6790	<0.0001*
A_{300}	−0.0032	0.0007	<0.0001*

[a]A negative β (standardized coefficient) indicates a negative relationship between the independent and dependent variables.
*Indicate significant values ($P < 0.05$).

methods (i.e., stratified clipping or leaf collection within traps), which can be destructive, or indirect methods based on radiative transfer theory, which require assumptions about light propagation within the canopy (Bréda, 2003; Jonckheere et al., 2004; Weiss et al., 2004). Vertical canopy depth, in turn, assumes a vertically stratified arrangement of the canopy, thus ignoring the three-dimensional nature of the canopy structure. Digitizing techniques, such as LiDAR, have shown exceptional promise as universal approaches for quantifying both environmental and biological variation within canopies at resolutions below the scale of individual leaves (Greaves et al., 2015; Magney et al., 2016; Swatantran et al., 2016). Recent LiDAR studies have provided new insights into canopy heterogeneity by coupling a ray-tracing algorithm with spatial coordinates to determine path length (Magney et al., 2016). This method, similar to our own calculation of R_D, requires determining the distance from the canopy exterior to a fixed point within the canopy interior. Our three-dimensional mapping approach, however, provides a less expensive and more portable alternative, capable of resolving canopy heterogeneity at a leaf-scale resolution. In addition, our method offers the ability to quantify leaf position within the interior of the canopy, a functionality not possible via LiDAR.

Although our three-dimensional mapping approach is inexpensive, easy to implement, and can provide detailed quantitative data regarding environmental and biological heterogeneity throughout the entirety of the canopy, this method is inherently built upon several assumptions. In particular, the method treats the trunk of the tree as a volume-less origin within the coordinate system. Although this treatment does not influence the quantification of φ, systematic errors in ρ and θ can occur. In addition, both the calculations of R_D and V_D rely on the assumption that the canopy shape is hemispherical, ignoring potential asymmetries or gaps within the canopy. Although R_D and V_D can be measured directly in the field, the determination of absolute depths would substantially increase the collection time of individual leaf parameters. The mathematical calculation of R_D and V_D, based on a hemispherical canopy model, can be executed rapidly across a large data set. In practice, the spherical polar coordinate system is best suited for small to medium hemispherical canopies that are easily accessible. However, for larger canopies or taller trees, the protractors could be repositioned to multiple locations within the canopy. Sampling data sets could then be mathematically merged using measured distances between sampling origin points. In addition, while our approach does not provide information regarding individual leaf angles, it can easily be coupled with similar inexpensive/portable methods capable of quantifying leaf angle (Escribano-Rocafort et al., 2014) or used in combination with other sampling techniques.

Overall, we have demonstrated that three-dimensional mapping can be used to probe the structure-property relationships of both environmental (i.e., PAR) and biological (i.e., A_{300}) measurements. The significant negative correlation of R_D with both PAR and A_{300} in our study provides vital clues regarding how the canopy structure efficiently balances the need for photoprotection with the corresponding energetic cost of biosynthesis. Using the spherical polar coordinate system to quantify leaf position, however, is not limited to studying the relationship between light and pigments. This simple, inexpensive, and portable method can also be used to more thoroughly understand how plants are affected by and respond to any abiotic or biotic factor, including quantifying how intraplant variation in leaf or floral traits is linked to spatial patterns of herbivory, the colonization and proliferation of microbes, and the effectiveness of pollinators.

LITERATURE CITED

AGATI, G., C. GALARDI, E. GRAVANO, A. ROMANI, AND M. TATTINI. 2002. Flavonoid distribution in tissues of *Phillyrea latifolia* L. leaves as estimated by microspectrofluorometry and multispectral fluorescence microimaging. *Photochemistry and Photobiology* 76: 350–360.

AGATI, G., C. BRUNETTI, M. DI FERDINANDO, F. FERRINI, S. POLLASTRI, AND M. TATTINI. 2013. Functional roles of flavonoids in photoprotection: New evidence, lessons from the past. *Plant Physiology and Biochemistry* 72: 35–45.

BALDOCCHI, D. D., K. B. WILSON, AND L. GU. 2002. How the environment, canopy structure and canopy physiological functioning influence carbon, water and energy fluxes of a temperate broad-leaved decidous forest—an assessment with the biophysical model CANOAK. *Tree Physiology* 22: 1065–1077.

BEGGS, C. J., AND E. WELLMANN. 1994. Photocontrol of flavonoid biosynthesis. *In* R. E. Kendrick and G. H. M. Kronenberg [eds.], Photomorphogenesis in plants, ed. 2, 733–751. Kluwer Academic Publishers, Dordecht, The Netherlands.

BILGER, W., T. JOHNSEN, AND U. SCHREIBER. 2001. UV-excited chlorophyll fluorescence as a tool for the assessment of UV-protection by the epidermis of plants. *Journal of Experimental Botany* 52: 2007–2014.

BRÉDA, N. J. J. 2003. Ground-based measurements of leaf area index: A review of methods, instruments and current controversies. *Journal of Experimental Botany* 54: 2403–2417.

BURCHARD, P., W. BILGER, AND G. WEISSENBÖCK. 2000. Contribution of hydroxycinnamates and flavonoids to epidermal shielding of UV-A and UV-B radiation in developing rye primary leaves as assessed by ultraviolet-induced chlorophyll fluorescence measurements. *Plant, Cell & Environment* 23: 1373–1380.

CEN, Y.-P., AND J. F. BORNMAN. 1993. The effect of exposure to enhanced UV-B radiation on the penetration of monochromatic and polychromatic UV-B radiation in leaves of *Brassica napus. Physiologia Plantarum* 87: 249–255.

COCKELL, C. S., AND J. KNOWLAND. 1999. Ultraviolet radiation screening compounds. *Biological Reviews of the Cambridge Philosophical Society* 74: 311–345.

DAY, T. A., AND S. M. DEMCHIK. 1996a. Influence of enhanced UV-B radiation on biomass allocation and pigment concentrations in leaves and reproductive structures in greenhouse-grown *Brassica rapa. Vegetatio* 127: 109–116.

DAY, T. A., AND S. M. DEMCHIK. 1996b. Ultraviolet-B radiation screening effectiveness of reproductive organs in *Hesperis matronalis. Environmental and Experimental Botany* 36: 447–454.

DIXON, R. A., AND N. L. PAIVA. 1995. Stress-induced phenylpropanoid metabolism. *Plant Cell* 7: 1085–1097.

EL MORCHID, E. M., P. T. LONDOÑO, M. PAPAGIANNOPOULOS, L. GOBBO-NETO, AND C. MÜLLER. 2014. Variation in flavonoid pattern in leaves and flowers of *Primula veris* of different origin and impact of UV-B. *Biochemical Systematics and Ecology* 53: 81–88.

Ellsworth, D. S., and P. B. Reich. 1993. Canopy structure and vertical patterns of photosynthesis and related leaf traits in a deciduous forest. *Oecologia* 96: 169–178.

Escribano-Rocafort, A. G., A. B. Ventre-Lespiaucq, C. Granado-Yela, A. López-Pintor, J. A. Delgado, V. Muñoz, G. A. Dorado, and L. Balaguer. 2014. Simplifying data acquisition in plant canopies: Measurements of leaf angles with a cell phone. *Methods in Ecology and Evolution* 5: 132–140.

Everhart, S. E., A. Askew, L. Seymour, I. J. Holb, and H. Scherm. 2011. Characterization of three-dimensional spatial aggregation and association patterns of brown rot symptoms within intensively mapped sour cherry trees. *Annals of Botany* 108: 1195–1202.

Frederick, J. E., H. E. Snell, and E. K. Haywood. 1989. Solar ultraviolet radiation at the Earth's surface. *Photochemistry and Photobiology* 50: 443–450.

Greaves, H. E., L. A. Vierling, J. U. H. Eitel, N. T. Boelman, T. S. Magney, C. M. Prager, and K. L. Griffin. 2015. Estimating aboveground biomass and leaf area of low-stature Arctic shrubs with terrestrial LiDAR. *Remote Sensing of Environment* 164: 26–35.

Griffen, L. R., A. M. Wilczek, and F. A. Bazzaz. 2004. UV-B affects within-seed biomass allocation and chemical provisioning. *New Phytologist* 162: 167–171.

Hirose, T., and M. J. A. Werger. 1987. Maximizing daily canopy photosynthesis with respect to the leaf nitrogen allocation pattern in the canopy. *Oecologia* 72: 520–526.

Izaguirre, M. M., C. A. Mazza, A. Svatos, I. T. Baldwin, and C. L. Ballaré. 2007. Solar ultraviolet-B radiation and insect herbivory trigger partially overlapping phenolic responses in *Nicotiana attenuata* and *Nicotiana longiflora. Annals of Botany* 99: 103–109.

Jonckheere, I., S. Fleck, K. Nackaerts, B. Muys, P. Coppin, M. Weiss, and F. Baret. 2004. Review of methods for in situ leaf area index determination: Part I. Theories, sensors and hemispherical photography. *Agricultural and Forest Meteorology* 121: 19–35.

Kolb, C. A., M. A. Käser, J. Kopecký, G. Zotz, M. Riederer, and E. E. Pfündel. 2001. Effects of natural intensities of visible and ultraviolet radiation on epidermal ultraviolet screening and photosynthesis in grape leaves. *Plant Physiology* 127: 863–875.

Landry, L. G., C. C. S. Chapple, and R. L. Last. 1995. *Arabidopsis* mutants lacking phenolic sunscreens exhibit enhanced ultraviolet-B injury and oxidative damage. *Plant Physiology* 109: 1159–1166.

Le Roux, X., A. S. Walcroft, F. A. Daudet, H. Sinoquet, M. M. Chaves, A. Rodriques, and L. Osorio. 2001. Photosynthetic light acclimation in peach leaves: Importance of changes in mass:area ratio, nitrogen concentration, and leaf nitrogen partitioning. *Tree Physiology* 21: 377–386.

Li, J., T. M. Ou-Lee, R. Raba, R. G. Amundson, and R. L. Last. 1993. *Arabidopsis* flavonoid mutants are hypersensitive to UV-B irradiation. *Plant Cell* 5: 171–179.

Li, T., E. Heuvelink, T. A. Dueck, J. Janse, G. Gort, and L. F. M. Marcelis. 2014. Enhancement of crop photosynthesis by diffuse light: Quantifying the contributing factors. *Annals of Botany* 114: 145–156.

Lois, R. 1994. Accumulation of UV-absorbing flavonoids induced by UV-B radiation in *Arabidopsis thaliana. Planta* 194: 498–503.

Lovelock, C. E., B. F. Clough, and I. E. Woodrow. 1992. Distribution and accumulation of ultraviolet-radiation-absorbing compounds in leaves of tropical mangroves. *Planta* 188: 143–154.

Madronich, S. 1993. The atmosphere and UV-B radiation at ground level. *In* A. R. Young, L. O. Björn, J. Moan, and W. Nultsch [eds.], Environmental UV photobiology, pp. 1–39. Plenum Press, New York, New York, USA.

Magney, T. S., J. U. H. Eitel, K. L. Griffin, N. T. Boelman, H. E. Greaves, C. M. Prager, B. A. Logan, et al. 2016. LiDAR canopy radiation model reveals patterns of photosynthetic partitioning in an Arctic shrub. *Agricultural and Forest Meteorology* 221: 78–93.

Mazza, C. A., H. E. Boccalandro, C. V. Giordano, D. Battista, A. L. Scopel, and C. L. Ballaré. 2000. Functional significance and induction by solar radiation of ultraviolet-absorbing sunscreens in field-grown soybean crops. *Plant Physiology* 122: 117–126.

McKee, K. L. 1995. Interspecific variation in growth, biomass partitioning, and defensive characteristic of neotropical mangrove seedlings: Response to light and nutrient availability. *American Journal of Botany* 82: 299–307.

Nascimento, L. B. S., M. V. Leal-Costa, E. A. Menezes, V. R. Lopes, M. F. Muzitano, S. S. Costa, and E. S. Tavares. 2015. Ultraviolet-B radiation effects on phenolic profile and flavonoid content of *Kalanchoe pinnata. Journal of Photochemistry and Photobiology. B, Biology* 148: 73–81.

Pierce, L. L., and S. W. Running. 1988. Rapid estimation of coniferous forest leaf area index using a portable integrating radiometer. *Ecology* 69: 1762–1767.

Reuber, S., J. F. Bornman, and G. Weissenböck. 1996. A flavonoid mutant of barley (*Hordeum vulgare* L.) exhibits increased sensitivity to UV-B radiation in the primary leaf. *Plant, Cell & Environment* 19: 593–601.

Room, P. M., J. S. Hanan, and P. Prusinkiewicz. 1996. Virtual plants: New perspectives for ecologists, pathologists and agricultural scientists. *Trends in Plant Science* 1: 33–38.

Schnitzler, J.-P., T. P. Jungblut, W. Heller, M. Köfferlein, P. Hutzler, U. Heinzmann, E. Schmelzer, et al. 1996. Tissue localization of U.V.-B-screening pigments and of chalcone synthase mRNA in needles of Scots pine seedlings. *New Phytologist* 132: 247–258.

Sinoquet, H., B. Moulia, and R. Bonhomme. 1991. Estimating the three-dimensional geometry of a maize crop as an input of radiation models: Comparison between three-dimensional digitizing and plant profiles. *Agricultural and Forest Meteorology* 55: 233–249.

Sinoquet, H., S. Thanisawanyangkura, H. Mabrouk, and P. Kasemsap. 1998. Characterization of the light environment in canopies using 3D digitising and image processing. *Annals of Botany* 82: 203–212.

Sullivan, J. H., D. G. Gitz III, L. Liu-Gitz, C. Xu, W. Gao, and J. Slusser. 2007. Coupling short-term changes in ambient UV-B levels with induction of UV-screening compounds. *Photochemistry and Photobiology* 83: 863–870.

Swatantran, A., H. Tang, T. Barrett, P. DeCola, and R. Dubayah. 2016. Rapid, high-resolution forest structure and terrain mapping over large areas using single photon lidar. *Scientific Reports* 6: 28277.

Tattini, M., E. Gravano, P. Pinelli, N. Mulinacci, and A. Romani. 2000. Flavonoids accumulate in leaves and glandular trichomes of *Phillyrea latifolia* exposed to excess solar radiation. *New Phytologist* 148: 69–77.

Tegelberg, R., R. Julkunen-Tiitto, and P. J. Aphalo. 2001. The effects of long-term elevated UV-B on the growth and phenolics of field-grown silver birch (*Betula pendula*). *Global Change Biology* 7: 839–848.

Tevini, M., J. Braun, and G. Fieser. 1991. The protective function of the epidermal layer of rye seedlings against ultraviolet-B radiation. *Photochemistry and Photobiology* 53: 329–333.

Valladares, F. 2003. Light heterogeneity and plants: From ecophysiology to species coexistence and biodiversity. *In* K. Esser, U. Lüttge, W. Beyschlag, and F. Hellwig [eds.], Progress in botany, 439–471. Springer Verlag, Berlin, Germany.

Weinig, C., K. A. Gravuer, N. C. Kane, and J. Schmitt. 2004. Testing adaptive plasticity to UV: Costs and benefits of stem elongation and light-induced phenolics. *Evolution* 58: 2645–2656.

Weiss, M., F. Baret, G. J. Smith, I. Jonckheere, and P. Coppin. 2004. Review of methods for in situ leaf area index (LAI) determination: Part II. Estimation of LAI, errors and sampling. *Agricultural and Forest Meteorology* 121: 37–53.

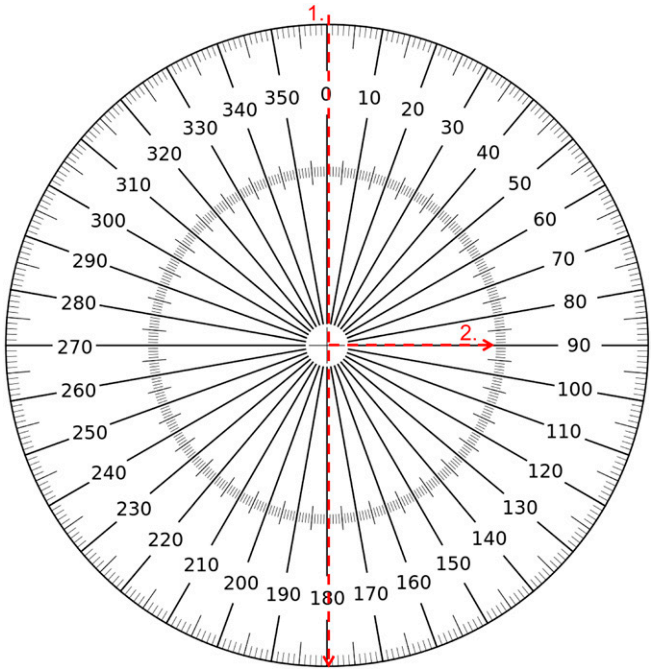

Appendix 1. Zenith angle (θ) protractor construction template. Appropriate cuts and their respective orders are indicated by the dashed lines and numbers. Image reproduced from https://commons.wikimedia.org/wiki/File:Rapporteur.svg#filelinks (Rapporteur.svg, Autiwa) under a CC BY-SA 3.0 license (https://creativecommons.org/licenses/by-sa/3.0/legalcode). Overlaid images by J. D. Patterson.

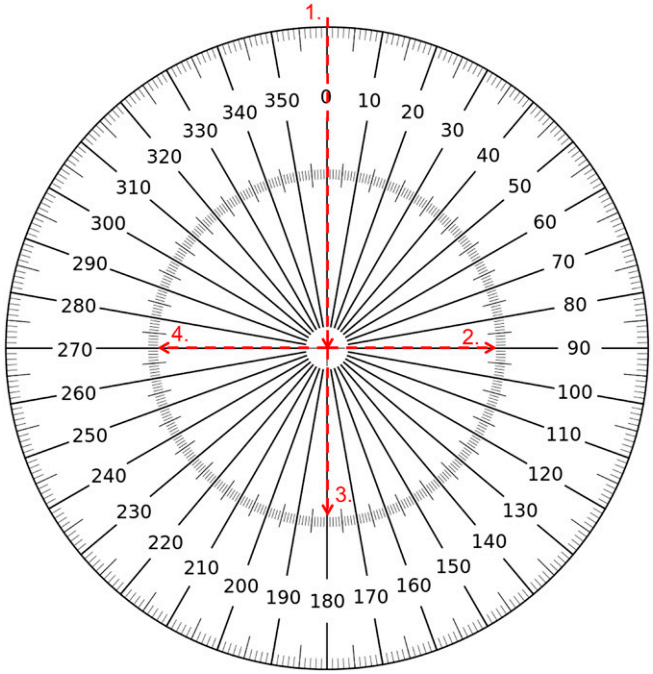

Appendix 2. Azimuthal angle (φ) protractor construction template. Appropriate cuts and their respective orders are indicated by the dashed lines and numbers. Image reproduced from https://commons.wikimedia.org/wiki/File:Rapporteur.svg#filelinks (Rapporteur.svg, Autiwa) under a CC BY-SA 3.0 license (https://creativecommons.org/licenses/by-sa/3.0/legalcode). Overlaid images by J. D. Patterson.

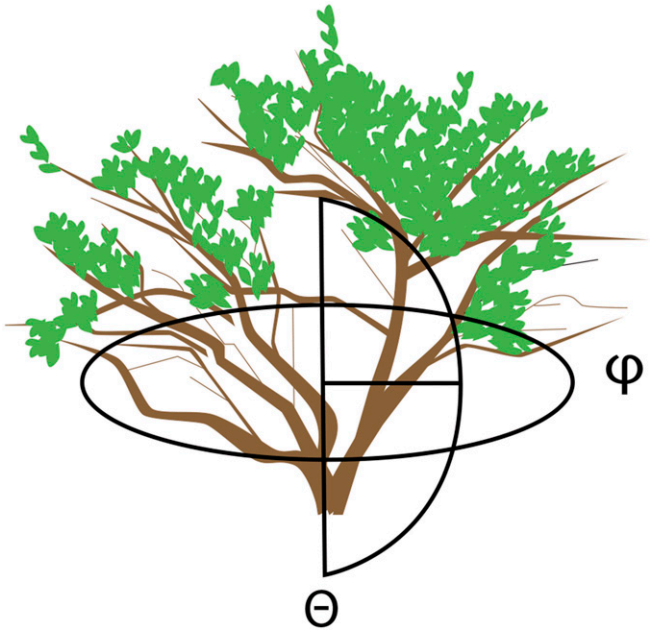

Appendix 3. Schematic illustrating the arrangement of the zenith (θ) protractor and azimuthal (φ) protractor at the base of the canopy.